

Modeling of surface roughness effects on Stokes flow in circular pipes

Cite as: Phys. Fluids **30**, 023604 (2018); <https://doi.org/10.1063/1.5017876>

Submitted: 01 December 2017 . Accepted: 01 February 2018 . Published Online: 16 February 2018

Siyuan Song, Xiaohu Yang, Fengxian Xin , and Tian Jian Lu



View Online



Export Citation



CrossMark

ARTICLES YOU MAY BE INTERESTED IN

Publisher's Note: "Modeling of surface roughness effects on Stokes flow in circular pipes" [Phys. Fluids **30**, 023604 (2018)]

Physics of Fluids **30**, 049901 (2018); <https://doi.org/10.1063/1.5029966>

Drag reduction induced by superhydrophobic surfaces in turbulent pipe flow

Physics of Fluids **30**, 025102 (2018); <https://doi.org/10.1063/1.5011805>

Characterization of surface roughness effects on pressure drop in single-phase flow in minichannels

Physics of Fluids **17**, 100606 (2005); <https://doi.org/10.1063/1.1896985>

PHYSICS TODAY
WHITEPAPERS

ADVANCED LIGHT CURE ADHESIVES

Take a closer look at what these environmentally friendly adhesive systems can do

READ NOW

PRESENTED BY
 **MASTERBOND**
ADHESIVES | SEALANTS | COATINGS



Modeling of surface roughness effects on Stokes flow in circular pipes

Siyuan Song,^{1,2} Xiaohu Yang,^{1,3} Fengxian Xin,^{1,2,a)} and Tian Jian Lu^{1,2,b)}

¹MOE Key Laboratory for Multifunctional Materials and Structures, Xi'an Jiaotong University, Xi'an 710049, China

²State Key Laboratory for Strength and Vibration of Mechanical Structures, Xi'an Jiaotong University, Xi'an 710049, China

³School of Human Settlements and Civil Engineering, Xi'an Jiaotong University, Xi'an 710049, China

(Received 1 December 2017; accepted 1 February 2018; published online 16 February 2018; corrected 6 March 2018)

Fluid flow and pressure drop across a channel are significantly influenced by surface roughness on a channel wall. The present study investigates the effects of periodically structured surface roughness upon flow field and pressure drop in a circular pipe at low Reynolds numbers. The periodic roughness considered exhibits sinusoidal, triangular, and rectangular morphologies, with the relative roughness (i.e., ratio of the amplitude of surface roughness to hydraulic diameter of the pipe) no more than 0.2. Based upon a revised perturbation theory, a theoretical model is developed to quantify the effect of roughness on fully developed Stokes flow in the pipe. The ratio of static flow resistivity and the ratio of the Darcy friction factor between rough and smooth pipes are expressed in four-order approximate formulations, which are validated against numerical simulation results. The relative roughness and the wave number are identified as the two key parameters affecting the static flow resistivity and the Darcy friction factor. *Published by AIP Publishing.* <https://doi.org/10.1063/1.5017876>

I. INTRODUCTION

Fluid flow in pipes is a fundamental problem in science and engineering. The pioneering work goes back to Poiseuille,¹ who conducted a series of experiments on pipe flow and found that the pressure gradient was proportional to the fourth power of hydraulic radius. Such flow behavior, named as the Poiseuille law, has become a basic property of pipe flow. Nowadays, with the assumption of a smooth and no-slip boundary, one can readily obtain solutions of fully developed laminar flow in a wide range of pipes that match well with experimental measurements.

In practice, the assumption of smooth boundary is often challenged by the fact that surface roughness is inevitable, especially for fluid flow in micro-channels. For instance, for fluid transport in porous media, cardiovascular systems, and micro-electro-mechanical systems (MEMSs), various microstructures (i.e., surface roughness) covering solid wall surfaces are encountered, which significantly affect the flow field. As a result, studying the influence of surface roughness on fluid flow has become necessary and important.

Surface roughness was identified as an important parameter governing pipe flow in the nineteenth century.² After a series of experiments on different rough pipes, Darcy established that the pressure drop through a rough pipe was correlated with its diameter and surface type by means of the Darcy friction factor,

$$f = \frac{\Delta p}{\frac{1}{2}\rho U^2 \frac{L}{D}}, \quad (1)$$

where Δp is the pressure drop, f is the Darcy friction factor, ρ is the fluid density, U is the average flow velocity, and D

and L are separately the hydraulic diameter and length of the pipe. Equation (1), known as the Darcy law, can be applied to analyze a known flow field, rather than calculate an unknown flow field. The friction factor, serving as an evaluation indicator, reflects the energy dissipation influenced by surface roughness, so one can utilize Eq. (1) to quantify the effect of surface roughness on pipe flow. A number of semi-empirical models on surface roughness effects have been developed over the decades.³ Further experimental studies indicated that the Reynolds number plays an important role,⁴ with three separate states of flow identified for the influence of surface roughness: laminar, transition, and turbulent flows. Based on extensive experimental studies, Colebrook and White⁵ and Colebrook⁶ obtained the well-known Colebrook equations that describe the correlation among the Darcy friction factor, the Reynolds number, and the relative roughness. Subsequently, making use of the Colebrook equations, Moody⁷ presented the famous Moody chart which has since been widely used in engineering.

According to existing research work, surface roughness (which was assumed to be composed of densely packed sand) had no direct effect on the friction factor in laminar flow ($Re < 2300$).⁸ Therefore, the Darcy friction factor can be expressed as⁹

$$f = \frac{Po}{Re}, \quad (2)$$

where Po is the Poiseuille number decided by the morphology of the pipe (channel).

Although the Colebrook equations led to good agreements with experimental results in some cases, a significant departure of the Darcy friction factor in the laminar flow regime was also observed according to recent experimental studies.^{10–13} Kandlikar *et al.*¹⁴ and Wagner and Kandlikar¹⁵ indicated that the real diameter of the channel should be replaced by the constricted flow diameter because of the flow constriction effect

a) Author to whom correspondence should be addressed: fengxian.xin@gmail.com

b) Author to whom correspondence should be addressed: tjlu@xjtu.edu.cn

(due to surface roughness) and verified their theoretical predictions by experiments. Zou *et al.*¹⁶ provided an in-depth analysis on the flow constriction effect and introduced a deviation coefficient to modify the conventional Darcy friction factor, as

$$f_{cf} = f \left[1 - \frac{2e}{D} \right]^{-4}, \quad (3)$$

where f_{cf} is the revised friction factor based on the constricted flow diameter, f is the conventional friction factor of Eq. (2), and e is the average roughness height. Equation (3) was built upon the assumption that surface roughness was relatively dense, and hence the equivalent diameter of the channel was constricted by the height of the roughness. Corresponding theoretical predictions of the pressure drop agreed with experimental results, and therefore it is reasonable and necessary to take the flow constriction effect into consideration. However, the assumption of flow constriction may cause discrepancy between theory and experiment when surface roughness is not so closely packed. In addition, existing theories only provide a simplified solution of pressure drop without detailed discussion of the flow field. From a theoretical point of view, as the distribution of velocity in a rough channel remains unknown, further exploitation of the roughness effect on the flow field and pressure drop is necessary.

Apart from the semi-empirical models as discussed above, a perturbation model has also been adopted to characterize surface roughness effects. For instance, with the Poiseuille flow in a smooth channel taken as the mean solution, the influence of surface roughness was considered as a perturbed term in the flow field.¹⁷ By solving the resulting perturbation equation, the distribution of the stream function in the flow field can be obtained. Bontozoglou and Papapolymerou¹⁸ presented a boundary perturbation model to calculate the laminar flow of a liquid down an inclined wall with sinusoidal corrugations, while Wang *et al.*¹⁹ solved the perturbation equation using the finite difference method and calculated, indirectly, the dependence of the Darcy friction factor on ribbon-like surface roughness. Nonetheless while these theories appeared to be rigorous and accurate in the prediction of velocity distribution, they did not consider the effect of flow constriction.

In the present research, we mainly study low-Reynolds-number flow (i.e., Stokes flow) in corrugated tubes, serving the basis for applications in biological systems, microfluidics, MEMS, and porous media, to name just a few. The rough surface of channels/pores in these fields plays an important role in energy dissipation and matter exchange. For instance, in biological systems, the movement of blood can be considered as creeping flow,²⁰ with the blood pressure seriously affected

by the microstructure grown on the vessel surface. Further, the compound vesicle under Stokes flow condition is a reasonable analogy of blood cell (i.e., erythrocyte, leukocyte, and platelet) inside the vessel.^{21–23} In microelectrical devices, heat sinks constructed on the basis of microchannels are often adopted for active cooling.²⁴ At large Reynolds numbers, a wavy (rough) boundary can enhance the heat transfer.^{25–27} By contrast, at sufficiently small Reynolds numbers, the wavy boundary may deteriorate the rate of heat transfer.²⁸ In the study of sound propagation across porous media, low-Reynolds-number is also a common assumption. Recently, it was demonstrated that roughness can promote viscous dissipation of sound energy by arrays of microslits having corrugated surfaces.²⁹

The main purpose of this study is to investigate theoretically the effect of surface roughness on fully developed Stokes flow by unifying three existing theoretical approaches: the Colebrook equations, the flow constriction model, and the perturbation model. A revised perturbation theory is developed to calculate the pressure drop and flow field in a circular pipe with periodic surface roughness. To quantify the overall deviation in velocity distribution due to the flow constriction effect, two dependent parameters are introduced and computed based on additional boundary conditions in extreme cases. Numerical simulations are performed to validate the proposed model.

II. CHARACTERIZATION OF SURFACE ROUGHNESS

Figure 1 illustrates schematically a circular pipe with periodic (sinusoidal) roughness placed on its inner wall. D is the hydraulic diameter of the pipe [i.e., the distance between the central axis of the sinusoidal roughness; Fig. 1(b)], e is the amplitude, and b is the wavelength of roughness. The length (L) of the pipe is considered to be sufficiently long to ensure fully developed flow. The periodic microstructures are treated as a kind of uniform surface roughness so that the boundary surface of the circular pipe can be described by

$$\bar{r} = \Gamma(x, \theta) D, \quad \text{with } \Gamma(x, \theta) = \frac{1}{2} - \varepsilon g(x), \quad (4)$$

where $(\bar{x}, \bar{r}, \theta)$ are the real coordinates, (x, r, θ) are the dimensionless coordinates with $x = \bar{x}/D$ and $r = \bar{r}/D$, $\Gamma(x, \theta)$ is the dimensionless boundary function, $\varepsilon = e/D$ is the relative roughness, and $g(x)$ is the surface morphology function. For simplicity, sinusoidal roughness is considered first so that

$$g(x) = \cos(\beta x), \quad (5)$$

where $\beta = 2\pi D/b$ is the wave number of roughness. Later, other types of roughness morphologies are also considered, including rectangular and triangular morphologies.

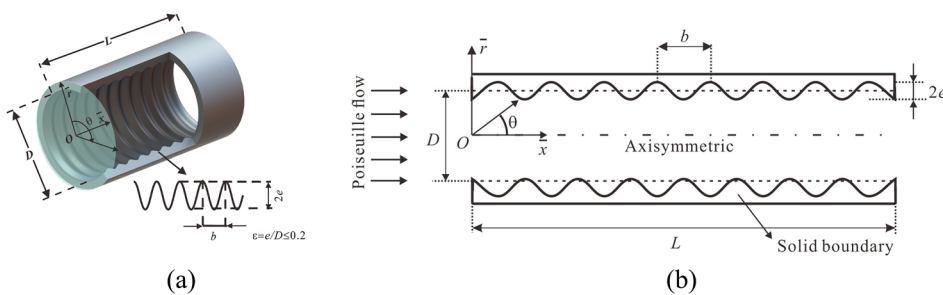


FIG. 1. Schematic of a circular pipe with periodic roughness on its inner surface: (a) three-dimensional view and (b) two-dimensional view.

III. ANALYSIS OF STATIC FLOW FIELD

A. Revised perturbation model

The revised perturbation theory is utilized to obtain the flow field in the circular pipe with surface roughness. Incompressible Newtonian fluid is considered, with fully developed steady laminar flow assumed. Further, to simplify the analysis, the Reynolds number is taken sufficiently small (e.g., $Re < 1$) so that Stokes flow is in force, with the inertia effect neglected. Here, ignoring the inertial term is considered acceptable^{30,31} because both the characteristic length and characteristic velocity are considerably small in the problem of Fig. 1. Malevich *et al.*³² calculated the fluid field of Stokes flow inside a channel with three-dimensional wavy walls. It was demonstrated that when the wave number of roughness is relatively small, no eddy could be formed. At sufficiently low Reynolds numbers, the nonlinear term in the governing function can be abandoned to obtain simplified solutions, instead of solving by a numerical method (e.g., finite difference method). Moreover, in the present study, small relative roughness (ranging from 0 to 0.2) is considered since a perturbation model is employed for modeling. Due to the linearity of the Stokes equations, it is feasible to adopt such a large range of relative roughness without significant loss of accuracy.

As shown in Fig. 1(b), the problem is axisymmetric and can be solved in two-dimensional (2D) cylindrical coordinates (\bar{x}, \bar{r}) . With periodicity considered, the analysis is performed in a characteristic element domain $\bar{x} \in (0, b)$, $\bar{r} \in (0, \Gamma(x, \theta)D)$. For fully developed steady incompressible flow, the non-dimensional Navier-Stokes equation is given by

$$0 = -\nabla p + \nabla^2 \mathbf{u}. \quad (6)$$

Subsequent analysis and calculation are all performed in the dimensionless fluid field.

The inner boundary of the rough pipe is assumed to be no-slip and no-penetration. The center line ($r = 0$) is considered to be axis-symmetric. Therefore, the boundary condition can be written as

$$\begin{cases} u = 0, v = 0, & \text{at } r = \Gamma(x, \theta), \\ u, v < \infty, & \text{at } r = 0, \end{cases} \quad (7)$$

where u and v are the axial and radial velocity component in the pipe, respectively. For incompressible fluid, the stream function ψ and the flow velocity components are linked by

$$u = \frac{1}{r} \frac{\partial \psi}{\partial r}, v = -\frac{1}{r} \frac{\partial \psi}{\partial x}. \quad (8)$$

Substitution of Eqs. (8) into Eq. (6) yields

$$E^2 E^2 (\psi) = 0, \quad (9)$$

where E^2 is the Stokes operator,³³ given by

$$E^2 = \frac{\partial^2}{\partial r^2} - \frac{1}{r} \frac{\partial}{\partial r} + \frac{\partial^2}{\partial x^2}. \quad (10)$$

Substituting the velocity of Eq. (8) into the boundary condition (7) leads to

$$\begin{cases} \frac{\partial \psi}{\partial x} = 0, \frac{\partial \psi}{\partial r} = 0, & \text{at } r = \Gamma(x, \theta), \\ \psi < \infty, & \text{at } r = 0. \end{cases} \quad (11)$$

Following Van Dyke,¹⁷ the stream function can be expressed as a combination of the basic solution for a smooth circular pipe plus a series of perturbed solutions. Thus, one can take the Taylor expansion of the stream function $\psi(x, r)$ about the small relative roughness ε and retain only its zero- and first-order terms,

$$\psi(x, r) = \psi_0(x, r) + \varepsilon \psi_1(x, r) + O(\varepsilon^2), \quad (12)$$

where $O(\varepsilon^n)$ is defined as the infinitesimal of the n -th order. According to the present model,

$$\psi(x, r)|_{r=\Gamma(x, \theta)} = \psi(x, r)|_{r=\frac{1}{2}} - \varepsilon g(x) \left(\frac{\partial \psi(x, r)}{\partial r} \right) \Big|_{r=\frac{1}{2}} + O(\varepsilon^2). \quad (13)$$

Note that, in Eq. (13), the complex boundary curve $r = \Gamma(x, \theta)$ has been taken equivalent to the simplified boundary curve $r = 1/2$. As a result, the influence of surface roughness is reflected by the first-order difference term $\varepsilon g(x) \left(\frac{\partial \psi(x, r)}{\partial r} \right) \Big|_{r=\frac{1}{2}}$. As a result, the following analysis and results are all deduced in the equivalent element domain $x \in (0, 2\pi/\beta)$, $r \in (0, 1/2)$.

Substitution of (12) into (9) leads to the following perturbation expansion of the Stokes equation:

$$E^2 E^2 (\psi_0) + \varepsilon E^2 E^2 (\psi_1) + O(\varepsilon^2) = 0. \quad (14)$$

Solving $E^2 E^2 (\psi_0) = 0$ gives the zero-order stream function $\psi_0 = r^2 - 2r^4$, corresponding to fully developed Poiseuille flow,

$$u_0 = 8(1/4 - r^2). \quad (15)$$

The first-order term of the perturbed equation together with the revised boundary condition are given by

$$\begin{cases} E^2 E^2 (\psi_1) = 0, \\ \frac{\partial \psi_1}{\partial x} = 0, \frac{\partial \psi_1}{\partial r} = -4g(x) + O(\varepsilon), & \text{at } r = \frac{1}{2}, \\ \psi_1 < \infty & \text{at } r = 0. \end{cases} \quad (16)$$

Traditionally, it has been suggested to solve Eq. (16) numerically, e.g., using the finite difference method.¹⁹ Nonetheless, the velocity field thus obtained leads to no growth in pressure drop along the roughened pipe, which is obviously inconsistent with experimental results.¹⁰⁻¹³ This is because the simplification of boundary conditions as detailed above leads to non-ignorable errors when the periodic roughness is densely distributed, that is, when the wave number β is relatively large. In reality, the surface roughness, serving as the disturbance source, causes significant nonlinearity at the boundary. Such nonlinearity magnifies the higher-order terms in the system so that the $O(\varepsilon)$ term in Eq. (16) cannot be neglected.

To address the aforementioned deficiency, one needs to modify the condition at the roughened boundary. Therefore, upon introducing a modification function $q(x, \varepsilon, \beta)$ to revise the boundary condition, the problem becomes

$$\begin{cases} E^2 E^2 (\psi_1) = 0, \\ \frac{\partial \psi_1}{\partial x} = 0, \frac{\partial \psi_1}{\partial r} = -4g(x) + q(x, \varepsilon, \beta), & \text{at } r = \frac{1}{2}, \\ \psi_1 < \infty & \text{at } r = 0. \end{cases} \quad (17)$$

The modification function $q(x, \varepsilon, \beta)$, which replaces $O(\varepsilon)$ in Eq. (16), depends on the position coordinate, relative roughness, and wave number of roughness. Nonetheless, at present,

the precise expression of $q(x, \varepsilon, \beta)$ is difficult to obtain, and it has been demonstrated that retaining more terms in the Taylor expansion of Eq. (13) does not work as well. Alternatively, an approximate estimation of $q(x, \varepsilon, \beta)$ is performed, as detailed below.

To simplify the present analysis of the surface roughness effect on pipe flow, let $Q(\varepsilon, \beta) = \int_0^{2\pi/\beta} q(x, \varepsilon, \beta) dx$, which represents the periodic average of flow constriction. To separate the two variables r and x in Eq. (17), take Fourier transform of the first-order term of the stream function in the x direction, as

$$\psi_1 = \sum_{k=-\infty}^{\infty} \varphi_k(r) e^{jk\beta x}. \quad (18)$$

Substitution of (18) into (17) yields

$$E^2 E^2 \left[\sum_{k=-\infty}^{\infty} \varphi_k(r) e^{jk\beta x} \right] = 0, \quad (19)$$

$$\begin{cases} \frac{\partial \psi_1}{\partial x} = 0, & \frac{\partial \psi_1}{\partial r} = -2e^{j\beta x} - 2e^{-j\beta x} + Qe^0, & \text{at } r = \frac{1}{2}, \\ \psi_1 < \infty & \text{at } r = 0. \end{cases}$$

According to this boundary condition, three terms ($k = -1, 0, 1$) remain in the expansion of the first-order stream function, namely,

$$\psi_1 = \varphi_1(r) e^{j\beta x} + \varphi_{-1}(r) e^{-j\beta x} + \varphi_0(r). \quad (20)$$

Here, $\varphi_1(r) e^{j\beta x}$ and $\varphi_{-1}(r) e^{-j\beta x}$ represent the periodic fluctuation of flow velocity along the axial direction, which have no direct effect on the growth of pressure gradient, while $\varphi_0(r)$ represents the overall deviation of flow velocity along the radial direction, which is responsible for increased pressure drop according to Eq. (6). Therefore, Eq. (17) can be separated into two independent governing functions, i.e., the fluctuation function and the deviation function, as

$$\left(\frac{\partial^2}{\partial r^2} - \frac{1}{r} \frac{\partial}{\partial r} - \beta^2 \right) \left(\frac{\partial^2}{\partial r^2} - \frac{1}{r} \frac{\partial}{\partial r} - \beta^2 \right) \varphi_1 = 0, \quad (21)$$

$$\begin{cases} \varphi_1 = 0, & \frac{\partial \varphi_1}{\partial r} = -2, & \text{at } r = \frac{1}{2}, \\ \varphi_1 < \infty, & & \text{at } r = 0, \end{cases}$$

$$\left(\frac{\partial^2}{\partial r^2} - \frac{1}{r} \frac{\partial}{\partial r} \right) \left(\frac{\partial^2}{\partial r^2} - \frac{1}{r} \frac{\partial}{\partial r} \right) \varphi_0 = 0, \quad (22)$$

$$\begin{cases} \frac{\partial \varphi_0}{\partial r} = Q, & \text{at } r = \frac{1}{2}, \\ \varphi_0 < \infty, & \text{at } r = 0. \end{cases}$$

The solution of (21) for the fluctuation function is detailed in the Appendix. Due to symmetry of the equation, φ_1 and φ_{-1} are complex conjugate. As previously discussed, this solution does not cause any increase in the pressure gradient.

As a key in understanding the influence of roughness on the pressure gradient, the solution to (22) for the deviation function is given by

$$\varphi_0(r) = \frac{M}{2} r^2 + \frac{N}{4} r^4, \quad (23)$$

where $M(\varepsilon, \beta)$ and $N(\varepsilon, \beta)$ are two functions that depend on relative roughness and wave number, satisfying $4M + N = 8Q$.

Further, with the consideration of flow conservation in an element domain $x \in (0, 2\pi/\beta)$, $r \in (0, 1/2)$, the velocity flux increment of incompressible fluid in this domain should be zero, namely, the volume integration of the first-order velocity u_1 equals zero,

$$\int_0^{2\pi/\beta} \int_0^{1/2} u_1 r dr dx = 0,$$

with

$$u_1 = \frac{1}{r} \left(\frac{d\varphi_0}{dr} + \frac{d\varphi_1(r)}{dr} e^{j\beta x} + \frac{d\varphi_{-1}(r)}{dr} e^{-j\beta x} \right). \quad (24)$$

The integration of the last two terms on the right-hand side of u_1 equals zero due to the integration property of trigonometric functions (i.e., $\int_0^{2\pi/\beta} e^{j\beta x} dx = 0$, $\int_0^{2\pi/\beta} e^{-j\beta x} dx = 0$). Inserting (23) into (24) yields

$$M = -8N. \quad (25)$$

Thus, there remains only one unknown parameter in (23). However, due to nonlinearity at the boundary, the conventional perturbation theory cannot precisely calculate M , N , or Q . Consequently, in Sec. III B, an approximate approach is proposed to determine M and N .

B. Solution

Given that surface roughness hinders fluid flow in pipes, one can quantify the hindering effect, albeit approximately, based on flow fields in two extreme cases as shown schematically in Fig. 2.

One limit is given by Eq. (3), valid only when the wave number of the sinusoidal surface roughness is very large (i.e., $\beta \rightarrow \infty$), as considered in the constricted flow model.^{14,15} Another limit corresponds to very small wave numbers ($\beta \rightarrow 0$). Consideration of the two extreme cases leads to two limiting values of pressure drop, i.e., the lower and upper bounds. As the wave number is increased, it becomes more difficult for the fluid to flow through the boundary layer. Given a specified relative roughness ε , it is expected that $\frac{\partial^2 p}{\partial x \partial \beta} < 0$, which results in $\frac{\partial}{\partial \beta} (\nabla^2 u_1) < 0$. This leads to $\frac{\partial}{\partial \beta} \left[\nabla^2 \left(\frac{1}{r} \frac{\partial \varphi_0}{\partial r} \right) \right] < 0$, finally yielding $\frac{\partial N}{\partial \beta} < 0$ [deduced from Eqs. (6), (10), (20), and (23)]. In other words, $N(\beta)$ is a

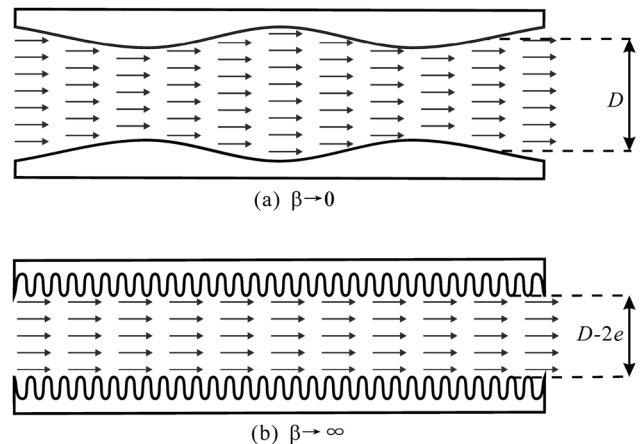


FIG. 2. Two extreme cases of a pipe with periodic surface roughness: (a) very small wave number ($\beta \rightarrow 0$) and (b) very large wave number ($\beta \rightarrow +\infty$).

decreasing function. For the problem considered in the current study, the logistic function³⁴ commonly adopted to describe an S-shaped growth curve satisfies all the properties of $N(\beta)$. Further, the growth ratio and limits of the logistic function depend in general on extreme cases. Therefore, the logistic function is used to approximate the dependence of M and N on β , as follows:

$$M = \left(M_1 \frac{2e^{-\frac{1}{5\pi}\beta}}{1 + e^{-\frac{1}{5\pi}\beta}} + M_2 \right), \quad (26)$$

$$N = \left(N_1 \frac{2e^{-\frac{1}{5\pi}\beta}}{1 + e^{-\frac{1}{5\pi}\beta}} + N_2 \right), \quad (27)$$

where M_1 , M_2 , N_1 , N_2 are four coefficients depending on relative roughness.

With reference to Fig. 2(b), when $\beta = \infty$, the flow field can be calculated approximately using the Poiseuille flow in a smooth pipe with diameter $(1 - 2\varepsilon)$, as

$$u_{\beta=\infty} = \frac{1}{2(0.5 - \varepsilon)^4} \left[(0.5 - \varepsilon)^2 - r^2 \right] \quad (28)$$

which yields

$$M_2 = \frac{1}{\varepsilon} \left[\frac{1}{2(0.5 - \varepsilon)^2} - 2 \right], \quad (29)$$

$$N_2 = \frac{1}{\varepsilon} \left[-\frac{1}{2(0.5 - \varepsilon)^4} + 8 \right]. \quad (30)$$

Similarly, based on Fig. 2(a), when $\beta \rightarrow 0$, the partial derivative of the flow velocity with respect to x is a higher-order infinitesimal term, i.e., $\frac{du}{dx} = \frac{du}{dr}$. The flow field can then be calculated approximately using the Poiseuille flow in a smooth pipe with varying diameter $(1 - 2\varepsilon \cos(\beta x))$, as

$$u_{\beta=0} = \frac{6(r - \varepsilon \cos(\beta x))(1 - \varepsilon \cos(\beta x) - r)}{1 - 6\varepsilon \cos(\alpha x) + 12\cos^2(\beta x)\varepsilon^2 - 8\cos^3(\beta x)\varepsilon^3} \quad (31)$$

from which one obtains

$$M_1 = \frac{2}{\varepsilon} \left(\frac{1}{(1 - 4\varepsilon^2)^{1.5}} - \frac{1}{(1 - 2\varepsilon)^2} \right), \quad (32)$$

$$N_1 = \frac{8}{\varepsilon} \left[\frac{1}{(1 - 2\varepsilon)^4} - \frac{(6\varepsilon^2 + 1)}{(1 - 4\varepsilon^2)^{3.5}} \right]. \quad (33)$$

The Stokes equation in the x direction can be rewritten as

$$\left(\frac{\partial^2}{\partial r^2} + \frac{1}{r} \frac{\partial}{\partial r} + \frac{\partial^2}{\partial x^2} \right) u = \frac{dp}{dx}. \quad (34)$$

The ratio of the average pressure drop (i.e., area-weighted average of dp/dx) across a rough pipe to that across a smooth pipe can be obtained as

$$k_{\text{sine}} = \frac{(\Delta p/L)_{\text{rough}}}{(\Delta p/L)_{\text{smooth}}} = 1 - \frac{\varepsilon N}{8}. \quad (35)$$

As an important parameter quantifying the influence of surface roughness on pressure drop, k_{sine} has been widely used to characterize fluid flow across roughened pipes. For example, the static flow resistivity, which evaluates the viscous resistivity of a pipe, is given by

$$\sigma = \frac{-\Delta p}{UL}. \quad (36)$$

The ratio of static flow resistivity between rough and smooth pipes can be weighed using k_{sine} , as

$$\frac{\sigma_{\text{rough}}}{\sigma_{\text{smooth}}} = \frac{(\Delta p/LU)_{\text{rough}}}{(\Delta p/LU)_{\text{smooth}}} = k_{\text{sine}}. \quad (37)$$

Similarly, the ratio of the Darcy friction factor between rough and smooth pipes can be obtained as

$$\frac{f_{\text{rough}}}{f_{\text{smooth}}} = \frac{[(2D\Delta p/L)/\rho U^2]_{\text{rough}}}{[(2D\Delta p/L)/\rho U^2]_{\text{smooth}}} = k_{\text{sine}}. \quad (38)$$

To determine k_{sine} , the function $N(\varepsilon, \beta)$ needs to be calculated. To this end, Eqs. (27), (30), (33), and (35) are combined to obtain

$$k_{\text{sine}} = \frac{1}{(1 - 2\varepsilon)^4} - \left(\frac{1}{(1 - 2\varepsilon)^4} - \frac{(6\varepsilon^2 + 1)}{(1 - 4\varepsilon^2)^{3.5}} \right) \frac{2e^{-\frac{1}{5\pi}\beta}}{1 + e^{-\frac{1}{5\pi}\beta}}, \quad (39)$$

which is valid when the relative roughness is small, e.g., $\varepsilon < 0.2$. Note that, when $\varepsilon \rightarrow 0$, both Eqs. (35) and (42) degrade to the fundamental solution $k_{\text{sine}} = 1$ although this is not so obvious from Eq. (42).

For the two extreme cases considered in Fig. 2, the solutions of k_{sine} are given by

$$k_{\text{sine}} = \frac{(6\varepsilon^2 + 1)}{(1 - 4\varepsilon^2)^{3.5}} \quad \text{at } \beta = 0, \quad (40)$$

$$k_{\text{sine}} = \frac{1}{(1 - 2\varepsilon)^4} \quad \text{at } \beta = \infty.$$

C. Rectangular and triangular surface roughness

In addition to sinusoidal roughness considered in Secs. III A and III B, other types of periodic surface roughness with, e.g., rectangular and triangular morphologies, can also be treated by decomposing their morphology function $g(x)$ into a series of sinusoidal functions via Fourier transform.

Figure 3 displays three different kinds of periodic surface roughness, with identical relative roughness and wave number. According to Eq. (16), the effect of roughness morphology on flow is characterized using the revised boundary condition.

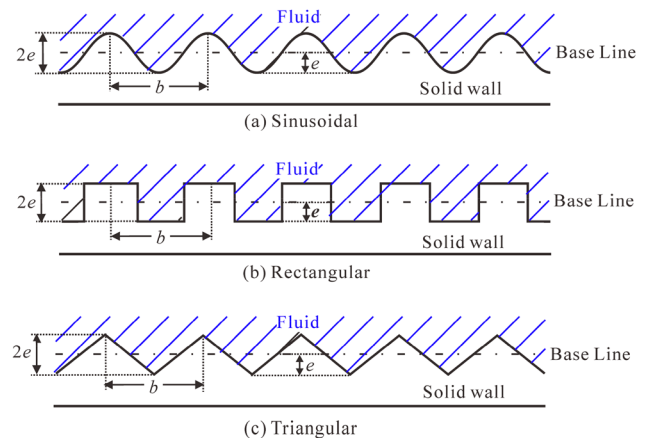


FIG. 3. (a) Sinusoidal, (b) rectangular, and (c) triangular roughness periodically distributed on the channel wall with identical relative roughness and wave number.

In view of the linearity of Eq. (9), the influence of rectangular or triangular roughness can be considered equivalent to that of a series of sinusoidal roughness upon Fourier transform.

The Fourier transforms of periodic rectangular and triangular roughness are given by

$$g_{\text{rectangle}}(x) = \frac{4}{\pi} \left[\cos(\beta x) - \frac{1}{3} \cos(3\beta x) + \frac{1}{5} \cos(5\beta x) + \dots + (-1)^{n-1} \frac{1}{(2n-1)} \cos((2n-1)\beta x) \right], \quad (41)$$

$$g_{\text{triangle}}(x) = \frac{8}{\pi^2} \left[\cos(\beta x) + \frac{1}{9} \cos(3\beta x) + \frac{1}{25} \cos(5\beta x) + \dots + \frac{1}{(2n-1)^2} \cos((2n-1)\beta x) \right], \quad (42)$$

where $n = 1, 2, 3, \dots, \infty$. As a first-order approximation, keeping only the first term in the foregoing equations, one can establish equivalence between sinusoidal roughness and rectangular/triangular roughness. Consequently, in view of (35), it follows that

$$\begin{cases} k_{\text{rectangle}}(\varepsilon, \beta) \approx k_{\text{sine}}\left(\frac{4}{\pi}\varepsilon, \beta\right), \\ k_{\text{triangle}}(\varepsilon, \beta) \approx k_{\text{sine}}\left(\frac{8}{\pi^2}\varepsilon, \beta\right). \end{cases} \quad (43)$$

The solution shows that the pressure drop for rectangular corrugation is more than that for sinusoidal corrugation and the pressure drop for triangle is less. This conclusion is consistent with the previous studies done by Herwig *et al.*⁹ By studying the problem of laminar flow passing the rough channels with Q-type, S-type, and T-type elements (i.e., rectangular, wavy, and triangular roughness), they pointed out that the entropy production in the cavities between the rough elements is almost negligible. Instead, the entropy production is more likely to be concentrated in a small band along the heads of the single roughness elements. As a result, the decreasing area of the heads of the rough element will lead to the decreasing resistivity effect.

IV. RESULTS AND DISCUSSION

To validate the proposed model, direct numerical simulations are performed. Fully developed laminar flow of air in a rough pipe is studied. The physical properties of air are summarized in Table I.

Air flow in the rough pipe is solved with Fluent 6.3TM at $Re = 0.6872$. For the representative model of Fig. 4(a), the flow is simulated using the laminar and axisymmetric solver. In most cases, the length (L) of the representative pipe is large

enough to ensure that the flow is fully developed and there are at least four periodic roughness in the numerical model ($L \geq 4b$). To ensure numerical accuracy, mesh sensitivity is checked for each model. The numerical results are independent of the grid resolution, as verified by systemically varying the size of the grid. According to Fig. 4(c), grid independence is satisfied as long as the number of cells is larger than 10 000 or the corresponding characteristic length of the cell does not exceed 2.5×10^{-5} m. The absolute criterion of the system is set at less than 10^{-8} to ensure the convergence of each calculation.

A. Velocity distribution

Figure 5 displays the radial distributions of flow velocity within a fully developed region ($1 \text{ mm} < \bar{x} < 5 \text{ mm}$) of a roughened circular pipe ($D = 1 \text{ mm}$; $L = 18 \text{ mm}$; $\varepsilon = 0.1$; $\beta = 2\pi$), as obtained separately from the present perturbation-based theoretical model and the Computational Fluid Dynamics (CFD) simulation. The results are given in dimensionless form in accordance with the theoretical deductions. For reference, corresponding results for a smooth pipe without roughness are also presented. Two significant features of the velocity distribution shown in Fig. 5 are observed:

- (i) **Periodic fluctuation** (with extent denoted by a purple arrow) represents the periodic change of flow field along the axial direction, which is consistent with the periodic distribution of surface roughness;
- (ii) **Overall deviation** (with extent denoted by a blue arrow) indicates the difference in the average flow field between the roughened pipe and the smooth pipe, which is attributed to the flow constriction effect.

Conclusively speaking, the velocity field follows a wavy pattern. The phase of the periodic fluctuation is identical to the phase of wavy boundary [as shown in Eq. (20)], so the maximum of the periodic fluctuation is happening both at the corrugation peak and corrugation bottom. The amplitude of the periodic fluctuation is determined by the solution of Eq. (21). Figure 5 shows that the maximum amplitude occurs near the axisymmetric line ($r = 0$). The position (center line) of the periodic fluctuation is determined by Eq. (22), characterizing the overall deviation of the flow field.

More details are given in Fig. 6, which compares the flow field inside the rough tube with different wave numbers ($\beta = 0.4\pi, 2\pi, 10\pi$). Based on the cylinder coordinate, both the velocity contour and streamline diagram are plotted inside the rough tube. It shows that with the increase of the wave number, there are much less streamlines appearing inside the cavity between the two rough elements. When the wave number is large, the velocity field in the rough channel is similar to the velocity field in the corresponding smooth channel with reduced radius.

The results of Fig. 5 show that the present model predictions match well with the numerical results at $r = 0, 0.1, 0.2$, and 0.3 , while small deviations are found at $r = 0.4$ and 0.5 as the roughened wall is approached. The latter is mainly attributed to the fact that the disturbance source, $r = \Gamma(x, \theta)$, will amplify the relative error at the roughened wall. However, this should not undermine the application potential of

TABLE I. Physical parameters of air and geometric parameters of the circular pipe.

Physical parameter	Values
Density	$\rho = 1.23 \text{ kg/m}^3$
Dynamic viscosity	$\mu = 1.79 \times 10^{-5} \text{ Pa/s}$
Average velocity	$U = 0.01 \text{ m/s}$
Diameter	$D = 0.001 \text{ m}$

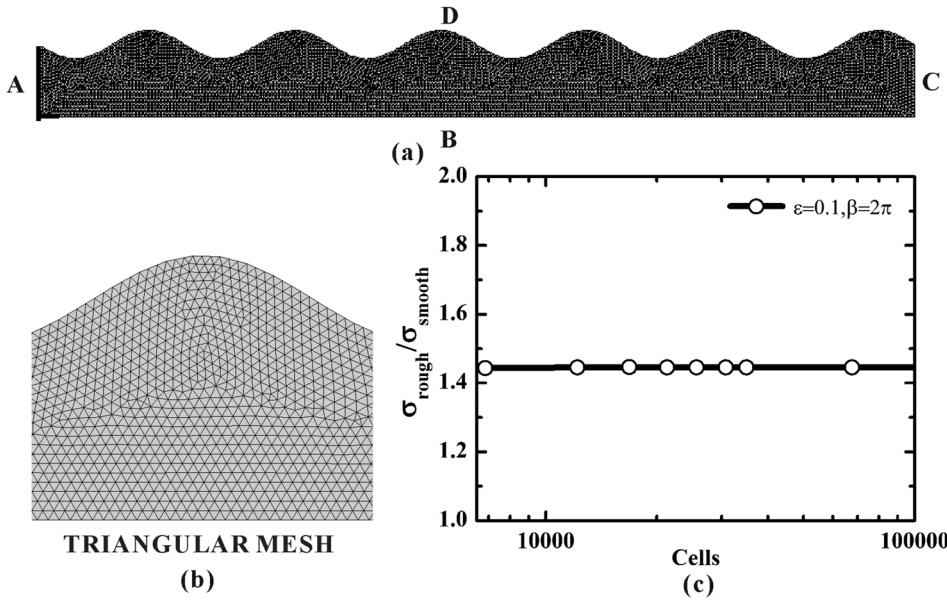


FIG. 4. Representative numerical model of fully developed air flow in (a) a roughened circular pipe ($\varepsilon = 0.1; \beta = 2\pi$) (A: velocity inlet; B: axis; C: outflow; D: wall); (b) triangular mesh; (c) grid independence tests based on the absolute value of relative static flow resistivity (i.e., $\sigma_{\text{rough}}/\sigma_{\text{smooth}}$) versus the number of cells.

the proposed model. According to Figs. 5(a)–5(f), the model accurately predicts all the important features of the periodic velocity field, such as period, phase, amplitude, and central line, which makes it good enough to characterize the flow field in a roughened circular pipe. In Sec. IV B, another important parameter of the problem, the static flow resistivity, will be determined.

B. Static flow resistivity

Static flow resistivity is an important parameter that quantifies the viscous resistivity of a channel and has been widely

used in the characterization of porous media. With the flow constriction effect in a roughened circular pipe determined as shown in Secs. III and IV A, its static flow resistivity can be readily calculated. In Fig. 7, the theoretically predicted static flow resistivity of a roughened pipe, normalized by that of the corresponding smooth pipe, is compared with the CFD simulation results. Overall, good agreement is achieved.

According to Fig. 7(a) for the case of $D = 1$ mm; $\beta = 2\pi$, there exists an accelerated growth of the ratio of static flow resistivity $\sigma_{\text{rough}}/\sigma_{\text{smooth}}$ about relative roughness ε , even when ε is as large as 0.2. The results of Fig. 7(b) for the case

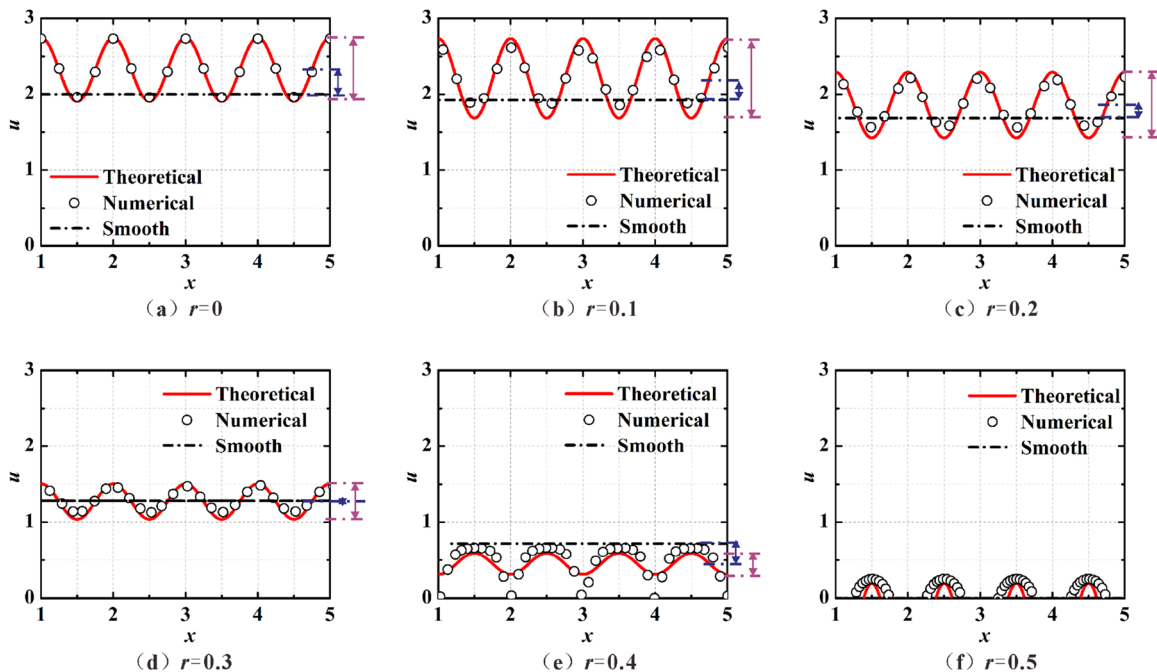


FIG. 5. Comparison of theoretical model predictions and CFD simulation results for radial distribution of dimensionless velocity u in a roughened circular pipe ($D = 1$ mm; $L = 18$ mm; $\varepsilon = 0.1; \beta = 2\pi$): (a) $u(x, r)|_{r=0}$; (b) $u(x, r)|_{r=0.1}$; (c) $u(x, r)|_{r=0.2}$; (d) $u(x, r)|_{r=0.3}$; (e) $u(x, r)|_{r=0.4}$; (f) $u(x, r)|_{r=0.5}$. Corresponding results for a smooth circular pipe are presented for reference.

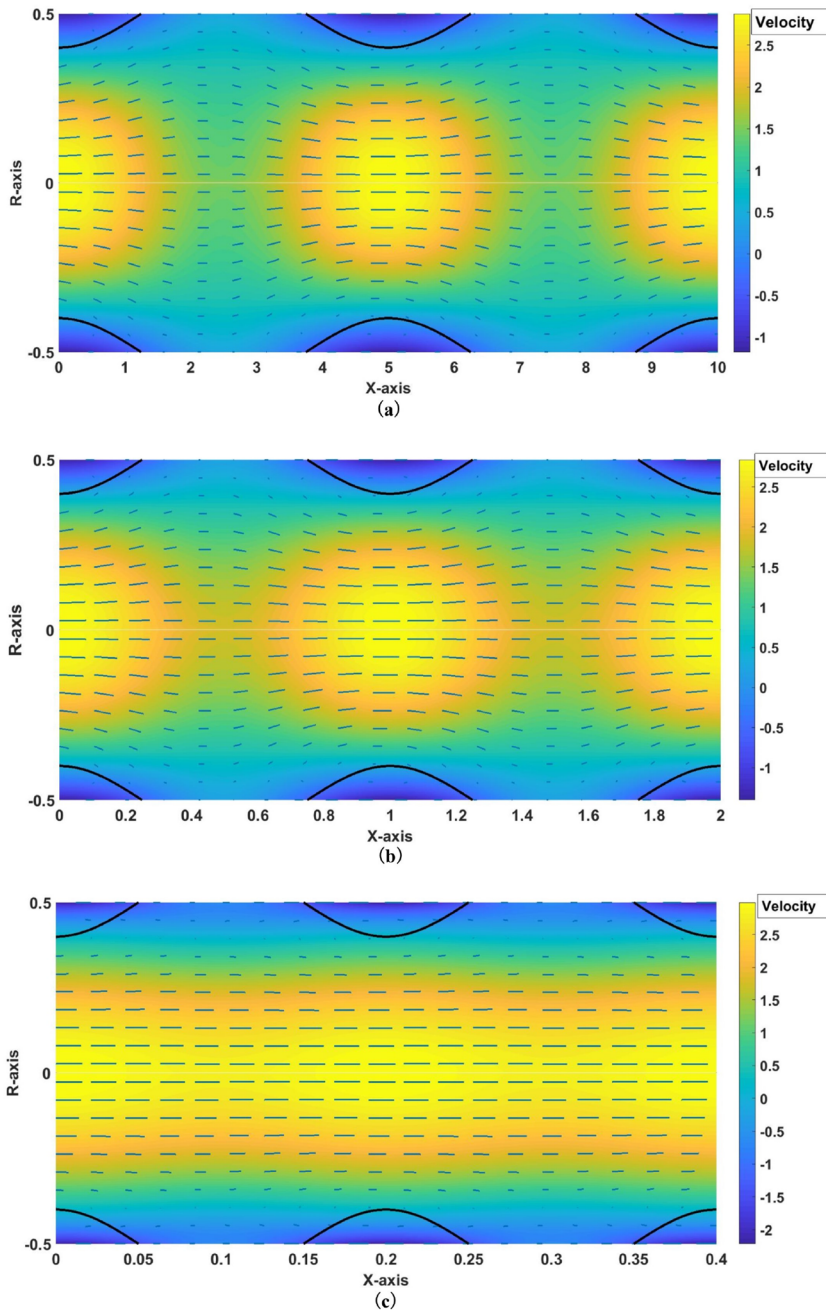


FIG. 6. Velocity contour and streamline of the flow field: (a) $\beta = 0.4\pi$; (b) $\beta = 2\pi$; (c) $\beta = 10\pi$ ($\varepsilon = 0.1$).

of $D = 1$ mm, $\varepsilon = 0.1$ indicate that increasing the wave number of roughness leads to a significant increase in static flow resistivity, which is mainly caused by the increased surface area. When the wave number grows larger, the static flow resistivity

will converge to the solution of the equivalent smooth channel with the diameter of $(D - 2e)$, and any further change in wave number will not change the flow field and resistivity accordingly.

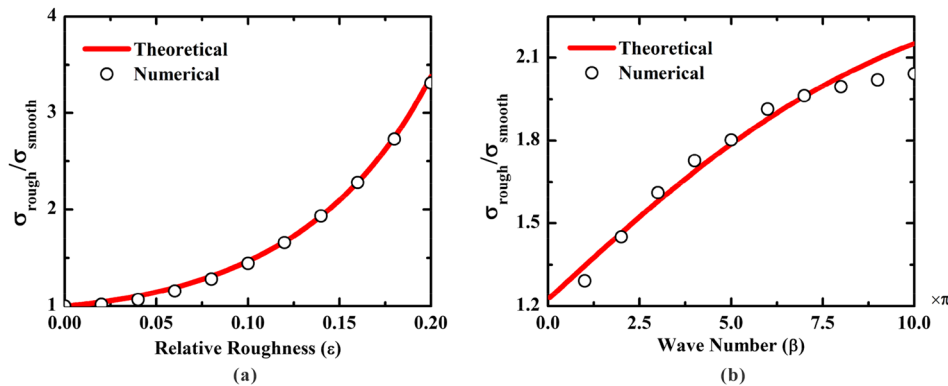


FIG. 7. Comparison of static flow resistivity between theoretical predictions and numerical calculations: (a) effect of relative roughness ($D = 1$ mm; $\beta = 2\pi$) and (b) effect of wave number ($D = 1$ mm; $\varepsilon = 0.1$).

Conclusively, the theoretical prediction agrees well with the numerical results. When the wave number becomes large, however, the numerically calculated static flow resistivity becomes smaller than the theoretical predictions, which can be explained using Eq. (28). When $\beta \rightarrow \infty$, the fluid flow domain is assumed to be blocked in the rough boundary region $r \in (0.5 - \varepsilon, 0.5 + \varepsilon)$. Under such conditions, using the analogue of the Poiseuille flow in a constricted channel, one can determine the flow field. However, the application of the Poiseuille flow is somewhat inappropriate here, for even when β is relatively large, the equivalent boundary $r = 0.5 - \varepsilon$ is still filled with fluid. It is more reasonable to employ the slip boundary condition at $r = 0.5 - \varepsilon$ instead of the no-slip boundary.¹⁴ Nonetheless, for typical wave numbers (e.g., $\beta < 10\pi$) as considered here, the error associated with the present theoretical prediction of static flow resistivity is relatively small.

C. Discussion

Figure 8 compares the Darcy friction factors calculated using Colebrook's equations, the constricted flow method, and the present model. The effect of relative roughness for the case of $D = 1$ mm, $\beta = 0\pi, 5\pi, 10\pi$ is displayed in Fig. 8(a), and the effect of wave number for the case of $D = 1$ mm, $\varepsilon = 0.1$ is presented in Fig. 8(b).

The results of Fig. 8 reveal that the revised perturbation theory presented in the present study is applicable in a wide range of ε and β values (e.g., $0 \leq \varepsilon \leq 0.2$, $0 \leq \beta < \infty$): when $\varepsilon \rightarrow 0$, the prediction degrades to the basic solution $f = \frac{64}{Re}$ of Colebrook's equations;⁹ when $\beta \rightarrow \infty$, the prediction degrades to $f = (1 - 2\varepsilon)^{-4} \frac{64}{Re}$ given by the constricted flow model.¹⁶ These limit properties, which have already been presented in Eq. (40), demonstrate the superiority of the present model.

Conventional theories of surface roughness effect are more or less associated with limitations: both Colebrook's equations and the constricted flow model fail to provide rigorous analysis of the effect of wave number because they are essentially built on the global fitting of experimental results; the conventional perturbation theory does not provide accurate predictions of the shear stress on the boundary, for it is built upon approximation analysis of the Navier-Stokes equations.

Even worse, the conventional perturbation theory ignores the nonlinearity of boundary condition and neglects $O(\varepsilon)$ terms in Eq. (16). As a result, while this method can predict the periodic fluctuation of flow velocity along the axial direction, it fails to capture the overall deviation of flow in the radial direction responsible for enhanced pressure drop.

On the contrary, as demonstrated in Fig. 5, the revised perturbation theory proposed in the present study cannot only predict the periodic fluctuation of flow in Eq. (21) but also the overall deviation of flow in Eq. (22) that reflects the concentration of flow field (thus the growth of pressure drop). In other words, the proposed model overcomes the deficiencies of conventional approaches to obtain more accurate predictions of a fully developed laminar flow field (and hence pressure drop) in a circular pipe having periodic surface roughness. This is considered the main novelty of the present study.

Figure 9 displays the ratio of pressure drop across a rough pipe to that across a smooth pipe calculated using the present model as well as the numerical method. Three types of surface roughness with identical relative roughness and wave number are considered, as shown in Fig. 3. The theoretical predictions agree well with the numerical results when the wave number is relatively small ($\beta < 5\pi$). Figure 9(a) reveals that rectangular roughness has more influence on pressure drop than either sinusoidal or triangular roughness because it can generate step flow, which prevents the flow propagating through the boundary area and hence increases viscous dissipation. Figure 9(b) shows that the approximation solution of (43) is valid only when the wall roughness are not closely packed, which is attributed to the approximation of the roughness morphology in Eqs. (41) and (42). However, it is possible to improve the prediction accuracy by modifying the approximation functions (i.e., the logistic function) in Subsection III B.

In view of Figs. 7 and 9, it is interesting to see that the effect of relative roughness (ε) is better predicted than the effect of wave number (β), which can be explained by the approximation analysis in Subsection III B. First, with ε fixed, the logistic function is used to fit $M(\beta)$ and $N(\beta)$ as functions of β which would, inevitably, lead to fitting errors. Second, once $M(\beta)$ and $N(\beta)$ are determined, no assumption is made in calculating $M(\varepsilon)$ and $N(\varepsilon)$. As a result, the predicted

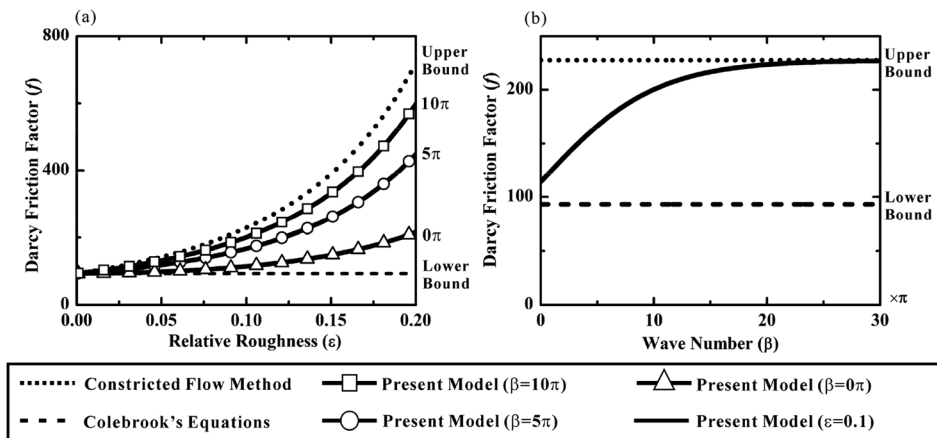


FIG. 8. Darcy friction factor predicted by using three different models: (a) effect of relative roughness ($D = 1$ mm; $\beta = 0\pi, 5\pi, 10\pi$) and (b) effect of wave number ($D = 1$ mm; $\varepsilon = 0.1$).

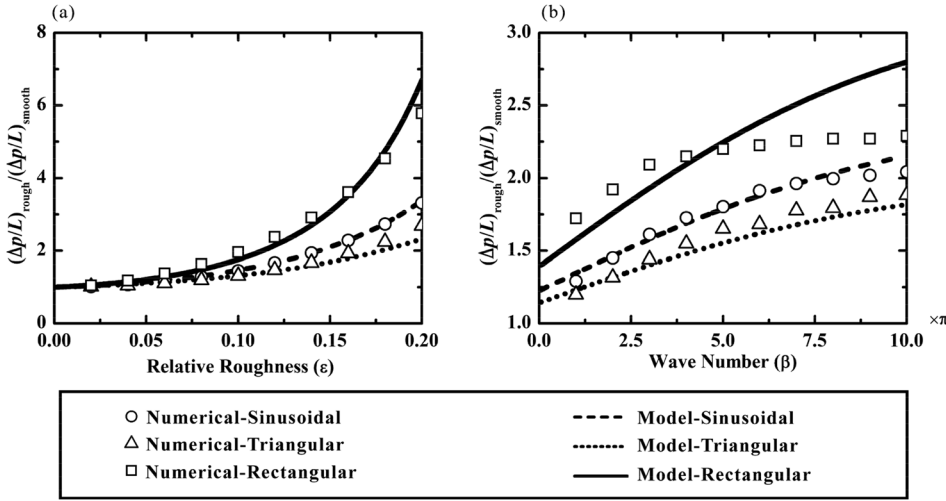


FIG. 9. Influence of roughness morphology on the pressure gradient: (a) effect of relative roughness ($D = 1$ mm; $\beta = 2\pi$) and (b) effect of wave number ($D = 1$ mm; $\epsilon = 0.1$).

relationship between the flow field and relative roughness can be accurate enough when we adopt the accurate $M(\beta)$ and $N(\beta)$ (at small wave number) to calculate $M(\epsilon)$ and $N(\epsilon)$, as shown in Figs. 7(a) and 9(a). By contrast, as shown in Figs. 7(b) and 9(b), the predicted flow field versus wave number relationship at a given relative roughness is less accurate. This also indicates that wave number is a key parameter in the analysis of roughness effect on pipe flow.

V. CONCLUSIONS

A theoretical model has been established to quantify the effect of periodic surface roughness on fully developed Stokes flow across a circular pipe by unifying three existing theoretical approaches (i.e., the Colebrook equations, the flow constriction model, and the perturbation model). Sinusoidal, rectangular, and triangular roughness morphologies with relatively small relative roughness ϵ and wave number β are considered. Approximated solutions of fluid flow and pressure drop are obtained and validated using direct numerical simulations. The main findings are as follows:

- The presence of periodic surface roughness leads to periodic fluctuation and overall deviation of fluid flow, which leads to growth in pressure drop.
- Increasing the relative roughness or wave number can increase pressure drop across a rough pipe, which is

predicted correctly by the present theory but not the previous theoretical methods.

- The predicted Darcy friction factor reduces, correctly, to $f = \frac{64}{Re}$ when $\epsilon \rightarrow 0$ and to $f = (1 - 2\epsilon)^{-4} \frac{64}{Re}$ when $\beta \rightarrow \infty$.
- With both ϵ and β fixed, rectangular roughness leads to a higher pressure gradient than sinusoidal or triangular roughness.

ACKNOWLEDGMENTS

This work was supported by the National Natural Science Foundation of China (Nos. 11761131003, 51528501, 11772248, and U1737107), and the Shaanxi Foundation for Selected Overseas Chinese (No. 2017025).

APPENDIX: SOLUTION OF THE PERIODIC FLUCTUATION FUNCTION

The governing equation in Eq. (21) can be rewritten as

$$\left[\frac{\partial^4}{\partial t^4} - \left(\frac{2}{t} \right) \frac{\partial^3}{\partial t^3} + \left(\frac{3}{t^2} - 2 \right) \frac{\partial^2}{\partial t^2} + \left(\frac{2}{t} - \frac{3}{t^3} \right) \frac{\partial}{\partial t} + 1 \right] \varphi_1 = 0,$$

where

$$t = \beta r. \quad (\text{A1})$$

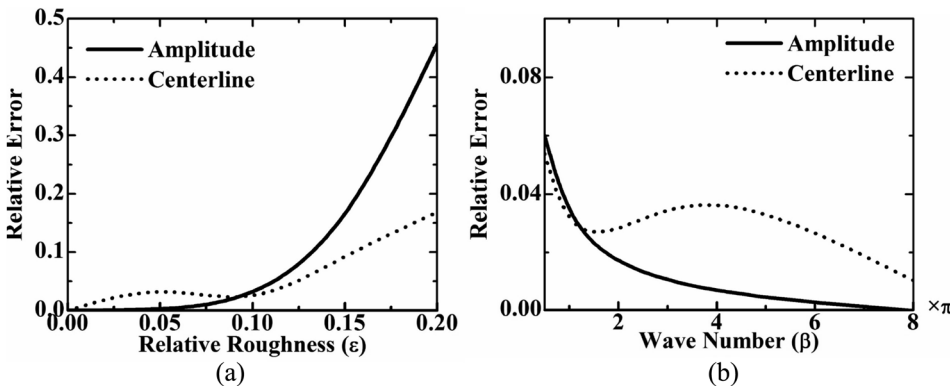


FIG. 10. Error analysis of the revised perturbation theory in the calculation of the value of the amplitude (i.e., periodic fluctuation) and the position of the centerline (i.e., overall deviation): (a) effect of relative roughness ($D = 1$ mm; $\beta = 2\pi$) and (b) effect of wave number ($D = 1$ mm; $\epsilon = 0.1$).

Based on the boundary condition $\varphi_1 < \infty$, at $t = 0$, the solution to Eq. (A1) is

$$\varphi_1(t) = \left\{ i^2 J(2, it) \right\} C_1 + \frac{1}{8} i \left\{ \pi t^3 J(0, it) J(2, it) Y(1, -it) + \pi t^3 J(0, it) J(1, it) Y(2, -it) \right\} C_3, \quad (\text{A2})$$

where $J_k(\beta t i)$ is the Bessel function of the k th-order and $Y_k(\beta t i)$ is the revised Bessel function of the k th-order. C_1, C_3 are two unknown constants that depend on the boundary condition

$$\varphi_1 = 0, \quad \frac{\partial \varphi_1}{\partial t} = -2, \quad \text{at } t = \frac{1}{2} \beta. \quad (\text{A3})$$

The proposed theory has already been validated by the numerical approach, as shown in Figs. 5, 7, and 9. To discuss the influence of the parameter on the relative error, an error analysis has been provided here, based on the calculation of the value of the amplitude (i.e., periodic fluctuation) and the position of the centerline (i.e., overall deviation).

According to Fig. 10(a), the relative error is growing with the increase of the relative roughness, due to the limitation of perturbation method. When $\varepsilon \geq 0.1$, the amplitude has a larger relative error than the position. As a result, at $\varepsilon = 0.2$, the results of the velocity field are no longer reliable, but the results of overall deviation and pressure drop still have considerable accuracy. According to Fig. 10(b), the decrease of the wave number can reduce the relative error. This is because when the wave number is large, most of the streamlines will concentrate on the center of the rough channel. The amplitude of the periodic fluctuation is approaching zero, leading to the decrease of relative error. In addition, since the overall deviation is calculated based on limit analysis, the relative error of overall deviation will be restricted in a reasonable range.

¹L. D. Landau and E. M. Lifshitz, *Fluid Mechanics*, 2nd ed. (Beijing World Publishing Corporation, China, 2008).

²H. Darcy, *Recherches Expérimentales Relatives au Mouvement de L'Eau dans les Tuyaux* (Mallet-Bachelier, France, 1857).

³J. B. Taylor, A. L. Carrano, and S. G. Kandlikar, "Characterization of the effect of surface roughness and texture on fluid flow-past, present, and future," *Int. J. Therm. Sci.* **45**(10), 962–968 (2006).

⁴J. Nikuradse, "Laws of flow in rough pipes," Report No. 1292, 1950.

⁵C. F. Colebrook and C. M. White, "Experiments with fluid friction in roughened pipes," *Proc. R. Soc. A* **161**(906), 367–381 (1937).

⁶C. F. Colebrook, "Turbulent flow in pipes with particular reference to the transition region between smooth and rough pipe laws," *J. Inst. Civ. Eng.* **11**(4), 133–156 (1939).

⁷L. F. Moody, "Friction factors for pipe flow," *Trans. ASME* **66**, 671–684 (1944).

⁸D. J. Schmitt and S. G. Kandlikar, "Effects of repeating microstructures on pressure drop in rectangular minichannels," in *ASME 3rd International Conference on Microchannels and Minichannels* (ASME, Toronto, Ontario, Canada, 2005), pp. 281–289.

⁹H. Herwig, D. Gloss, and T. Wenterodt, "A new approach to understanding and modelling the influence of wall roughness on friction factors for pipe and channel flows," *J. Fluid Mech.* **613**, 35–53 (2008).

¹⁰I. Papautsky, J. Brazzle, T. Ameal, and A. B. Frazier, "Laminar fluid behavior in microchannels using micropolar fluid theory," *Sens. Actuators, A* **73**(1), 101–108 (1999).

¹¹C. B. Sobhan and S. Garimella, "A comparative analysis of studies on heat transfer and fluid flow in microchannels," *Microscale Thermophys. Eng.* **5**(4), 293–311 (2001).

¹²G. Gamrat, M. Favre-Marinet, S. Le Person, R. Baviere, and F. Ayela, "An experimental study and modelling of roughness effects on laminar flow in microchannels," *J. Fluid Mech.* **594**, 399–423 (2008).

¹³W. Qu, G. M. Mala, and D. Li, "Pressure-driven water flows in trapezoidal silicon microchannels," *Int. J. Heat Mass Transfer* **43**(3), 353–364 (2000).

¹⁴S. G. Kandlikar, D. Schmitt, A. L. Carrano, and J. B. Taylor, "Characterization of surface roughness effects on pressure drop in single-phase flow in minichannels," *Phys. Fluids* **17**(10), 100606 (2005).

¹⁵R. N. Wagner and S. G. Kandlikar, "Effects of structured roughness on fluid flow at the microscale level," *Heat Transfer Eng.* **33**(6), 483–493 (2012).

¹⁶J. Zou, X. Peng, and W. Yan, "Effects of roughness on liquid flow behavior in ducts," in *ASME 2006 Joint U.S.-European Fluids Engineering Summer Meeting Collocated With the 14th International Conference on Nuclear Engineering* (ASME, USA, 2006), pp. 49–56.

¹⁷M. Van Dyke, *Perturbation Methods in Fluid Mechanics* (Parabolic Press, USA, 1964).

¹⁸V. Bontozoglou and G. Papapolymerou, "Laminar film flow down a wavy incline," *Int. J. Multiphase Flow* **23**(1), 69–79 (1997).

¹⁹H. Wang, Y. Wang, and J. Zhang, "Influence of ribbon structure rough wall on the microscale Poiseuille flow," *J. Fluids Eng.* **127**(6), 1140–1145 (2005).

²⁰R. Chadwick, "Slow viscous flow inside a torus—The resistance of small tortuous blood vessels," *Q. Appl. Math.* **43**(3), 317–323 (1985).

²¹T.-W. Pan, S. Zhao, X. Niu, and R. Glowinski, "A DLM/FD/IB method for simulating compound vesicle motion under creeping flow condition," *J. Comput. Phys.* **300**, 241–253 (2015).

²²J. Sohn, S. Li, X. Li, and J. S. Lowengrub, "Axisymmetric multicomponent vesicles: A comparison of hydrodynamic and geometric models," *Int. J. Numer. Methods Biomed. Eng.* **28**(3), 346–368 (2012).

²³J. S. Sohn, Y.-H. Tseng, S. Li, A. Voigt, and J. S. Lowengrub, "Dynamics of multicomponent vesicles in a viscous fluid," *J. Comput. Phys.* **229**(1), 119–144 (2010).

²⁴A. A. Koga, E. C. C. Lopes, H. F. V. Nova, C. R. de Lima, and E. C. N. Silva, "Development of heat sink device by using topology optimization," *Int. J. Heat Mass Transfer* **64**, 759–772 (2013).

²⁵L. Lin, J. Zhao, G. Lu, X.-D. Wang, and W.-M. Yan, "Heat transfer enhancement in microchannel heat sink by wavy channel with changing wavelength/amplitude," *Int. J. Therm. Sci.* **118**, 423–434 (2017).

²⁶A. G. Ramgadia and A. K. Saha, "Numerical study of fully developed flow and heat transfer in a wavy passage," *Int. J. Therm. Sci.* **67**, 152–166 (2013).

²⁷Z. G. Mills, A. Warey, and A. Alexeev, "Heat transfer enhancement and thermal-hydraulic performance in laminar flows through asymmetric wavy walled channels," *Int. J. Heat Mass Transfer* **97**, 450–460 (2016).

²⁸M. Vasudeviah and K. Balamurugan, "On forced convective heat transfer for a Stokes flow in a wavy channel," *Int. J. Heat Mass Transfer* **28**(2), 289–297 (2001).

²⁹S. Y. Song, X. H. Yang, F. X. Xin, S. W. Ren, and T. J. Lu, "Modeling of roughness effects on acoustic properties of micro-slits," *J. Phys. D: Appl. Phys.* **50**(23), 235303 (2017).

³⁰W. K.-H. Chu, "Stokes slip flow between corrugated walls," *Z. Angew. Math. Phys.* **47**(4), 591–599 (1996).

³¹C. Wang, "On Stokes slip flow through a transversely wavy channel," *Mech. Res. Commun.* **38**(3), 249–254 (2011).

³²A. Malevich, V. Mityushev, and P. Adler, "Stokes flow through a channel with wavy walls," *Acta Mech.* **182**(3), 151–182 (2006).

³³J. Happel and H. Brenner, *Low Reynolds Number Hydrodynamics*, 2nd ed. (Martinus Nijhoff Publishers, The Netherlands, 1983).

³⁴D. W. Hosmer and S. Lemesbow, *Applied Logistic Regression*, 2nd ed. (Wiley-Interscience, USA, 2000).